PROGRESS IN COLOR, COLORANTS AND COATINGS

available online @ www.pccc.icrc.ac.ir

Prog. Color Colorants Coat. 15 (2022), 157-174

Ministry of Science, Research and Technology
Institute for Color Science and Technology

Poly(amidoamine)-grafted Graphene Oxide/Epoxy Nanocomposite: Thermal/ Mechanical Characteristics and Viscoelastic Properties

M. Ganjaee Sari*, M. Rostami, S. Khamseh**

Faculty of Nanomaterials and Nanocoatings, Institute for Color Science and Technology (ICST), P.O. Box 16765-654, Tehran, Iran

ARTICLE INFO

Article history:
Received: 18 Apr 2021
Final Revised: 4 July 2021
Accepted: 06 July 2021
Available online: 06 Oct 2021

Keywords:
Epoxy
Nanocomposite coating
Graphene oxide
Surface modification
Mechanical properties.

ABSTRACT

As the most crucial choice in the heavy-duty protective coating industry, epoxy-based coatings suffer from insufficient toughness and impermeableness. So in this study, a reliable method that is, in turn, easy to be scaled up is designed and proposed. Through this method, a significantly toughened and mechanically improved epoxy nanocomposite film is suggested. This film is based on poly(amidoamine)-grafted (PAMAM) graphene oxide (GO). GO is synthesized and then modified through two consecutive steps; first, silane-grafted GO producing SiGO and second polyamidoamine (PAMAM)-grafted SiGO leading to HbpSiGO. FT-IR, TGA, and XRD results confirm a successful functionalization of the GO flakes. Dynamic mechanical thermal analysis (DMTA) results reveal that the nanocomposite film based on HbpSiGO possesses higher storage modulus (50 %), elevated glass transition temperature (18 %), and higher cross-linking density (237 %) compared to unfilled epoxy. According to tensile testing, HbpSiGO nanocomposite shows an increment in work of fracture (148%), elongation at break (52 %), and maximum stress (68 %) in comparison with neat epoxy. Prog. Color Colorants Coat. 15 (2022), 157-174© Institute for Color Science and Technology.

1. Introduction

Epoxy is one of the most widely used resins [1] that plays a critical role in different industries and has various applications [2-9]. Such diversified applicability is mainly because of its high tensile strength, high solvent and chemical resistance, excellent adhesion to many substrates, exceptional electrical properties, and the capability to be quickly processed [10].

Nevertheless, despite all these desired characteristics, epoxy exhibits some undesired mechanical properties like high brittleness, low toughness, and low impact resistance, making epoxy vulnerable in fracture mechanics and micro-cracks formation during service life [11, 12]. In addition, the effect of impregnating different fillers and additives on the mechanical reinforcement of the coatings has been reported by an enormous number of researchers [13-16].

It is now standard practice for researchers to exploit nanocomposite technology as an effective way to eliminate epoxy's weak points. At the same time, its advantages are simultaneously kept or even synergistically increased [17-19]. Furthermore, nanomaterials provide a very high specific surface area because of their tiny dimension size (below 100 nm), which offered numerous interfacial interactions with the medium; therefore, a small amount of them can result in significant changes. Therefore, graphene, as a two-dimensional and single-atom-thick structure with

*Corresponding author: * ganjaee-mo@icrc.ac.ir; ** rostami-m@icrc.ac.ir

extraordinary features, namely chemical inertness, thermal and chemical stability, high aspect ratio, and remarkable mechanical characteristics like high Young's modulus and work of fracture, seems to be a good choice for mechanical improvement [20].

Notwithstanding, such improvements are highly dependent on the state of particle dispersion and how strong they interfacially interact with the matrix [5]. Graphene lacks functional groups, and due to its chemical inertness, it cannot form a strong bonding with the matrix [21, 22]. However, the other graphene family members, i.e., graphene oxide (GO), have oxygenized functionalities such as epoxide and hydroxyl groups located frequently on the fundamental plane and carbonyl and carboxylic acid groups formed at the edge [20]. These functionalities alter the inertness of graphene into a hydrophilic nature and provide the possibility to tailor the final surface property of GO by substituting them with new chemical functionalities such as amino groups. The further substituents may interact physically and chemically with the matrix, leading to an improved homogenous stabilized dispersion and a maximized reinforcement. During the past few years, we have proposed some surface treatment and functionalization techniques [23-31] for improving the dispersion through increasing interfacial interactions of GO and other nanoparticles with the polymer matrix.

Alkoxysilane [11, 35-37] and hyperbranched polymers [38, 39] are used for surface modification among various methods [32-34], which have been reported. In addition, silane hybrid molecules have been designed in numerous structures with several functional groups that offer a simple substitution process through the renowned sol-gel mechanism at standard conditions.

On the other hand, hyperbranched polymers (HBP) belong to synthetic tree-like macromolecules and are known as dendritic polymers. Also, they provide a densely branched structure and many functional end groups with high chemical reactivity and enhanced solubility compared to their linear analogous. Besides, their viscosity diminishes as the degree of branches increases. This case also affects the polymer's relative solubility in various media. Therefore, By appropriate terminal groups of HBP, they can attach to the functionalities of GO via covalent linkage. Another distinct feature of HBP as a GO modifier is the capability of these polymers to diffuse into the GO galleries, increasing the stacks' d-spacing and hence better intercalation and exfoliation [34-36].

Researchers have conducted many studies on modifying graphene oxide to be used in resinous matrices, including epoxy polymers. However, few studies have been carried out in which the mechanical improvement of the resulted nanocomposite is assessed, and speculated mechanisms are suggested. Accordingly, in the current paper, it was decided to exploit the mentioned method to modify GO and investigate its effect on the mechanical characteristics of their nanocomposites. To this objective, GO was synthesized and then functionalized by (3-Glycidyloxypropyl) trimethoxysilane through the sol-gel process. In the next step, polyamidoamine (PAMAM) was chemically grafted to the functionalized GO from the previous step. Thus, the silane molecule can act as a coupling bridge between the hyperbranched polymer and GO. Afterward, the modified particles were dispersed in an epoxy resin and, the whole system was cured to prepare nanocomposite coatings. A schematic illustration of the final product structure, i.e., modified graphene oxide, is presented in Figure 1. Finally, mechanical properties (both dynamic and static modes) of the neat epoxy and nanocomposite counterparts are investigated and compared.

2. Experimental

2.1. Materials

Expandable graphite with particle size $d_{80\%} > 300$ μm, 98-99.5 % expansion rate, and density of 350-700 g/cm^3 was acquired from Kropfmühl Graphite Company. Synthesis-grade of $KMnO_4$, H_2O_2 (30 wt.%), H_2SO_4 (98 wt.%), and HCl (37 wt.%) from Millipore Sigma were used for the synthesis of graphene oxide. The silane precursor, i.e. (3-Glycidyloxypropyl) trimethoxysilane (GPTMS), with the chemical formula of $C_9H_{20}O_5Si$ (>98 wt%) and M_w of 236.34 g/mol was also acquired from Millipore Sigma company. Polyamidoamine (PAMAM) Hyperbranched polymer generation one, G1, was synthesized through the conventional convergent route. Ethylene diamine (EDA) was used as the core and methyl acrylate (MA) as the branching substances. The reaction contains two separate stages; first, EDA is reacted with MA to produce an ester-terminated outer layer. The product of this level is considered as generation zero, G0. Then, G0 is coupled with an appropriate amount of EDA to gain a new amino-

terminated surface. The product of this level is considered as generation one, G1. The nominal number of the amino-terminal group was calculated as eight groups per one molecule. Ethanol (99.6 % wt %) and toluene were gathered from Mojallali Co., Iran. Epoxy resin-based on Bisphenol-A diglycidyl ether (Epiran-01 X-75) was procured from Khuzestan Petrochemical Company. Polyamide-based curing agent, i.e., polyamide M-115x80, was provided by Manapolymer Co., Iran. Epoxide equivalent weight (EEW), epoxy group content, solid content, and viscosity at 25 °C of the epoxy resin were 434-555 g/eq, 0.189-0.230 mol/100g, 74-76 %, and 6000-12000 mPa.s, respectively. Amine number, solid content, density, and viscosity at 25 °C of the polyamide hardener were 210-250 mg KOH/gr, 80%, 0.96 kg/L, and 1100-1400 mPa.s, respectively.

2.2. Synthesis of graphene oxide (GO)

Graphene oxide was synthesized through a renowned route known as the modified Hummer method [26]. A brief of the way is as follows. First, graphite (0.5 g) was poured into a flask containing sulfuric acid (60 mL). The mixture was stirred continuously for 12 h to delaminate the graphite stacks of layers. Then, $KMnO_4$ (1.5 g) was gradually added and mixed for one h. This was carried out at temperatures below 20 °C. Afterward, the mixture was heated up to room temperature, and agitation was kept on for another 12 h. During this period, it is supposed that oxidation reactions of the graphene flakes start and accomplish. Then, purified water (600 mL) was poured into the flask to dilute the mixture while vigorous agitation was applied. Next, H_2O_2 (5 mL) was inserted into the mix to slow down and eventually stop the oxidation process. Next, The product was settled down by centrifuging and washed with 1 M HCl two times. Finally, it was rinsed with deionized water another three times. The resulting product is shown in Figure 2 (a).

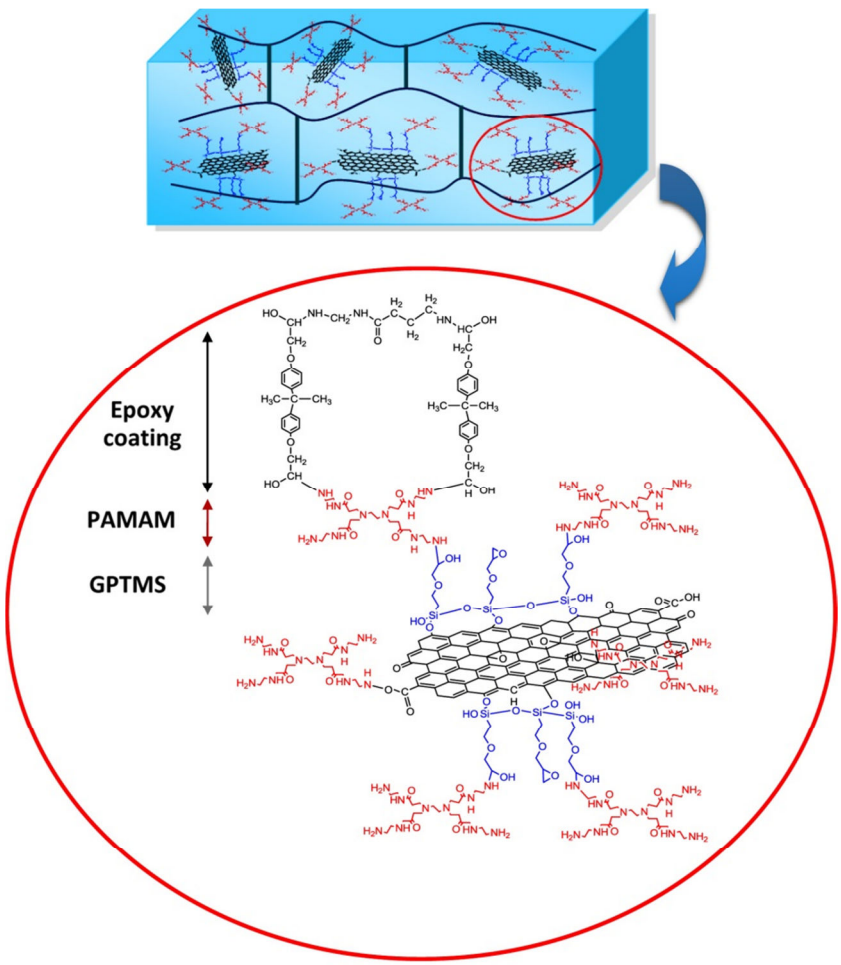

Figure 1: Schematic illustration of epoxy coating containing HbpSiGO nanosheets.

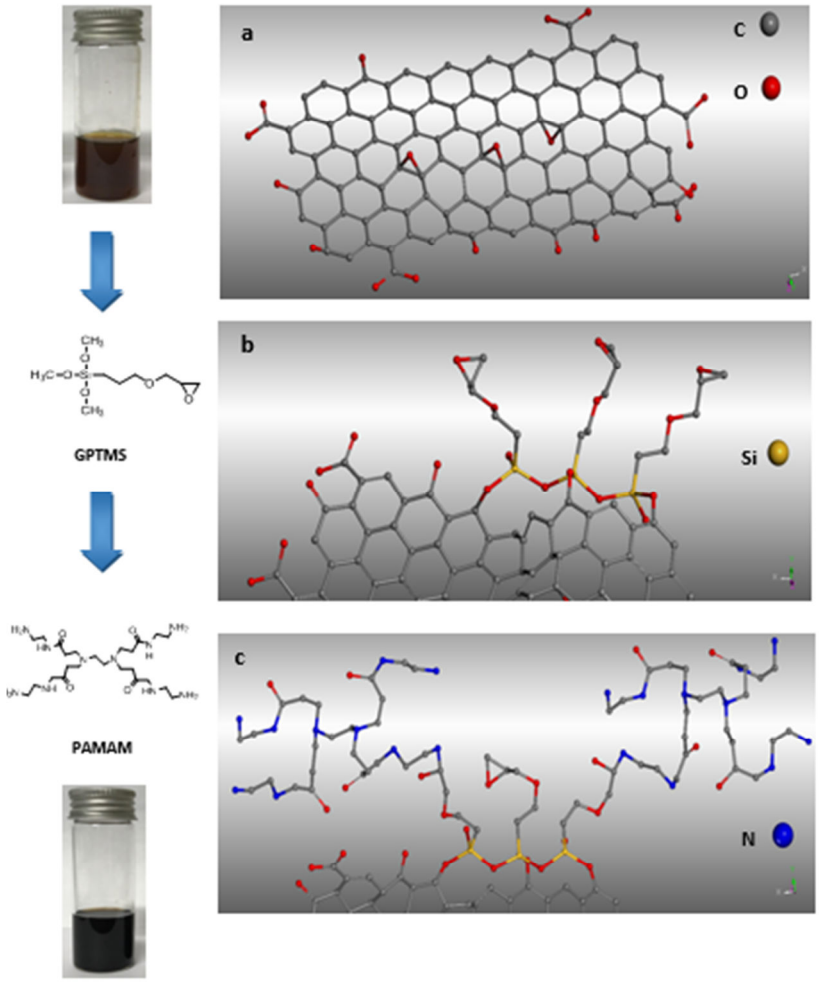

Figure 2: (a) GO, chemical grafting of GO with (b) GPTMS and (c) PAMAM.

2.3. Modification of GO by GPTMS

The functionalization of GO was carried out through the sol-gel method using (3-Glycidyloxypropyl) trimethoxysilane, i.e., GPTMS, as the silane precursor. For this procedure, the as-prepared aqueous suspension of GO was sonically re-dispersed for 5 min. Then, 0.25 g of GO was added to a three-neck flask containing 80 mL ethanol and 20 mL deionized (DI) water. The content pH was adjusted between 2 and 3 using few drops of hydrochloric acid 37 % to catalyze the hydrolysis reaction. Consequently, 5 mL of GPTMS was drop-wise poured into the flask while the whole system worked under reflux conditions. The mixture was then constantly agitated at a moderate rate for three h at 70 °C to ensure the hydrolysis reaction completion. Afterward, to catalyze the condensation reactions, pH was increased to values between 5 to 7 by adding a few drops of NaOH, and the stirring was continued for 24 hours. Eventually, the mixture was settled by centrifuging, and the product was washed four times by pure ethanol to eliminate physically adsorbed and loose silane molecules on the surface and unreacted silane in the medium. The chemical grafting of GPTMS with GO is shown in Figure 2 (b).

2.4. Modification of GPTMS-functionalized GO with PAMAM

GPTMS-functionalized graphene oxide, i.e., SiGO, and polyamidoamine hyperbranched polymer, i.e., PAMAM, were equally added to a three-neck flask containing 100 mL of pure ethanol to initiate the reactions between PAMAM amine and GPTMS glycidyl groups. So, The result production is PAMAM-modified SiGO, i.e., HbpSiGO. The process was carried out under reflux conditions and constant stirring. The temperature was adjusted to 70 °C, and

the operation lasted for 24 hours. The product was centrifugally settled and washed with pure ethanol four times to remove unreacted components to accomplish this process. Figure 2 (c) is depicted the chemical grafting of PAMAM with GPTMS functionalized GO.

2.5. Preparation of the nanocomposite coatings

For preparing the nanocomposite coatings, the particle suspensions must be undergone a solvent exchange process through which an epoxy-compatible solvent like toluene is replaced with water and ethanol. To this aim, the suspensions were centrifuged, and the upper-medium was thrown away, and toluene was altered. This was repeated several times to ensure all the water and ethanol are gone. Afterward, 0.1 wt.% of GO was added to the epoxy resin and mixed for three h at ambient temperature and 1000 rpm. Next, mixing was sonically augmented for 20 min at lowered power and frequency to eliminate chain degradation of the epoxy resin. Then, the resulting suspensions were mixed with a stoichiometric amount of curing agent, i.e., resin to hardener: 3 to 1 (w/w) accompanied with toluene as solvent. They were then applied on clean glass slides and kept in a cleanroom at room temperature for 24 hours. For a post-cure process, the films were held in an oven at 90 °C for one h to accomplish the curing reactions fully. Subsequently, cured free-standing films with a thickness of 40 ± five μm were obtained from these slides and safely kept for the following mechanical characterizing.

2.6. Particles characterization

FT-IR Spectroscopy evaluated the chemical composition of GO, SiGO, and HbpSiGO by using a Perkin-Elmer instrument across the wavenumbers of 4000 to 400 cm^{-1}. The structural changes were also investigated by XRD (Philips PW 1730) analysis across 5° to 80° with a step size of 0.05° and x-ray wavelength of 1.54065 Å. The x-ray was produced by a rotating anode tube of CuK_{α} radiation source. The obtained data were used to determine the interlayer distance, i.e., d_{001}. Thermal behavior was also studied using TGA spectra obtained by a Pyris 1 TGA Perkin Elmer Co. device within the temperature range of 25 to 750 °C in an N_2 environment. The analysis of Raman spectroscopy was also conducted using ExploRA™ PLUS HORIBA, Japan, with an excitation wavelength of 532 and 785 nm to study the structural defects. Changes in the hydrophobicity nature of the samples were assessed by measuring their contact angles with a water droplet. To do so, two μl of water was dripped onto the surface of the samples, and after 10 seconds, a close-up picture was recorded using a Canon digital camera. The morphology and elemental comparison of the samples were investigated exploiting FE-SEM, and EDS techniques carried out by a NOVA Nano SEM 450 instrument.

2.7. Mechanical properties characterizing

The mechanical characteristics of the nanocomposite coatings were assessed by a tensile test machine made by SANTAM modeled STM-5 (ASTM D638 & D3039). The extension rate was adjusted at 2 mm/min, and the tensile test for each sample was repeated five times. Dynamic mechanical analysis by DMTA-Triton, Tritec 2000 DMA instrument was performed at the frequency of 1 Hz. The temperature was ranged from -25 to 120 °C with a heating rate of 2 °C/min. The strain was adjusted at 0.02 % to ensure linear viscoelastic deformation of the samples**.**

3. Results and Discussion

3.1. Particles characterization

Calibrated FT-IR spectra for GO, SiGO, and HbpSiGO are depicted in Figure 3. As it is clear, GO shows the following characteristic peaks: O-H stretching at 3432 and 1378 cm^{-1}; C=O stretching at 1734 cm^{-1}; C=C in phenol at 1626 cm^{-1}; CH_2 at 2931 and 2847 cm^{-1}; C-O vibration in C-OH at 1224 cm^{-1}, and epoxide vibration at 1056 cm^{-1} [40-42]. These peak results approve the successful synthesis of graphene oxide. For SiGO, new peaks emerge at 585, 925, and 1115 cm^{-1}, which are assigned to asymmetric vibration and bending of Si-O-Si, Si-OH, and Si-O-C, respectively. A peak at 784 cm^{-1} related to the symmetric vibration of Si-O-Si also appears after functionalization of GO with GPTMS [43, 44]. The emergence of Si-O-C peak along with Si-O-Si and Si-OH is directly correlated to the silane molecules chemically attached to the functionalities of the GO flakes. Additionally, it is axiomatic that the peak intensity of CH_2 in SiGO has increased due to CH_2 groups of the GPTMS molecules. For HbpSiGO, a peak has emerged at 1560 cm^{-1} representing N-H of the amine groups of PAMAM, proving the existence of PAMAM molecules on the surface of the GPTMS-

modified GO.

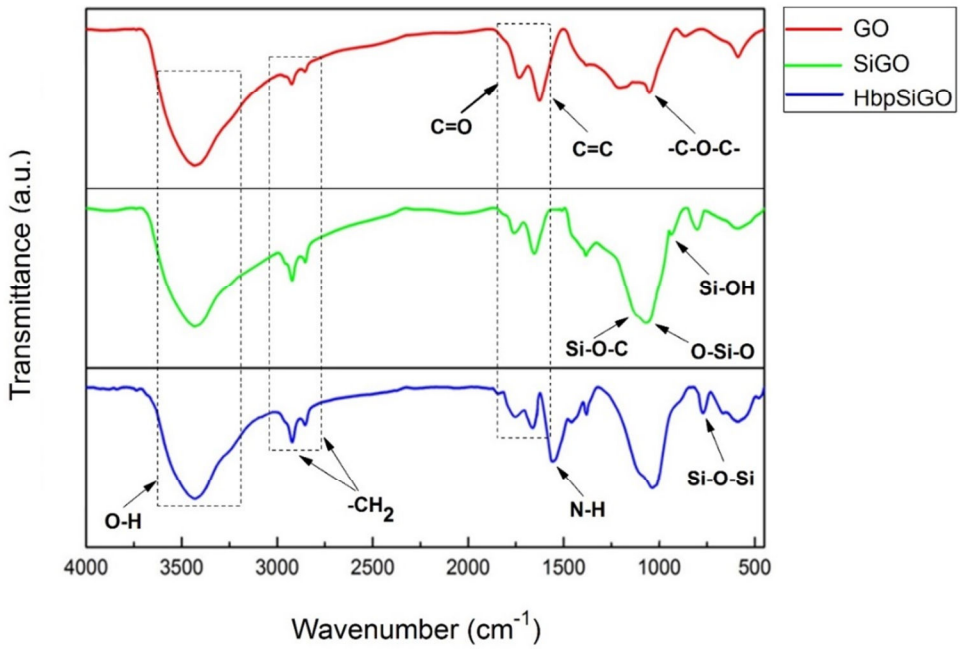

Figure 3: FT-IR spectra of GO, SiGO and HbpSiGO.

Successful grafting of GPTMS and PAMAM on the GO flakes was also sought by investigating the thermal behavior of the samples using TGA diagrams as depicted in Figure 4. The weight loss diagram of GO can be divided into three temperature regions: (1) the weight loss below 150 °C mostly related to the evaporation of water absorbed on the surface of GO; (2) the region in between 150 and 500 °C that is ascribed to the breakdown of functional groups of GO such as hydroxyl, carboxyl, and epoxide groups; and (3) the region across 500 to 700 °C that is associated to the disintegration of the carbon backbone of GO. The thermal behavior of GPTMS-modified Go and PAMAM-modified SiGO seems to be significantly different from GO itself.

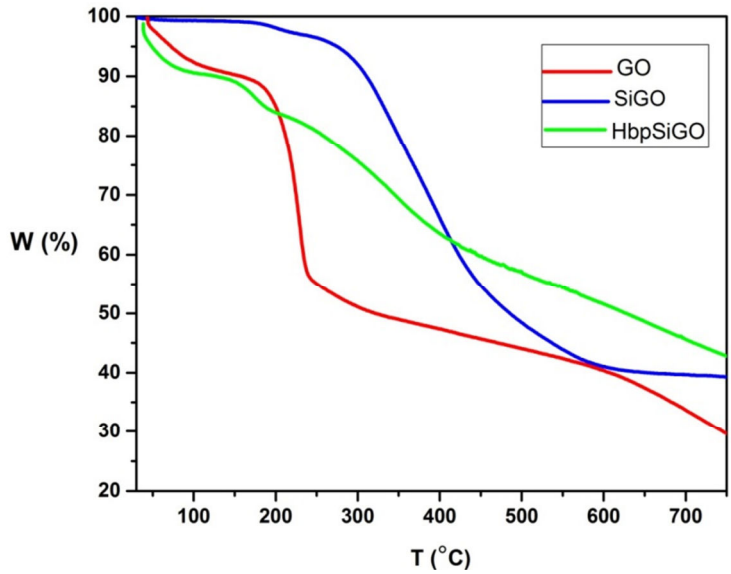

Figure 4: TGA diagrams of GO, SiGO and HbpSiGO.

To quantitatively compare the thermal behaviors, the data have been extracted from the diagrams and given in Table 1. The weight loss below 150 °C drastically drops from 7.54 % for GO to 0.42 % for SiGO, which declares adsorbed moisture significantly decreases as GPTMS modifies GO. This behavior can also be considered substantial evidence that approves the chemical attachment of GPTMS onto the GO flakes. These silane molecules are much more hydrophobic compared to GO and alter the hydrophilic nature of GO into a less hydrophilic one; therefore, water adsorption decreases. However, adding PAMAM molecules to the SiGO considerably increases hydrophilicity as the weight loss for HbpSiGO below 150 °C increases from 0.42 % for SiGO to 10.09 % HbpSiGO. This is also expected regarding the numerous amine groups of the PAMAM molecules. Across the span of 150 to 500 °C, the thermal behavior of the samples is different. While GO shows a significant drop at about 200 °C, HbpSiGO shows a much less steep reduction at about 300 °C. However, SiGO demonstrates a constant decreasing behavior for weight loss with a relatively small slope. Adding hybrid organic-inorganic GPTMS molecules has increased thermal stability compared to GO, and this enhancement deteriorates as the PAMAM molecules are inserted into the structure. Aside from the fact that all these behaviors are in good agreement with the components' chemical structures, the more important point is that TGA outcomes approve the chemical grafting of the GO flakes by both GPTMS and PAMAM. The overall conclusion from the TGA results is that the thermal stability of the SiGO and HbpSiGO have improved. This case can also be considered an indicator of the successful surface functionalization of GO.

To more profoundly pursue the structural changes due to the grafting reactions, Raman analysis can be helpful, as well. The D band and G band of a Raman spectrum are considered two distinctive peaks in graphene-containing systems. The D band demonstrates the presence of defects in the carbon skeleton of graphene that indicates the presence of sp^3 hybridization in the structure. This peak appears at 1338 cm^{-1} for GO. Therefore, intensity alteration and displacement of the peak may be used as an excellent clue to pursue structural changes.

On the other hand, the G band is attributed to sp^2 carbon hybridization and is observed at 1590 cm^{-1} in the spectrum. Accordingly, the ratio of D to G bands (I_D/I_G) as a calibrated dimensionless index somehow gives clues on the internal structure, which may lead to a better understanding of the effect of the surface grafting on the graphene oxide structure [45, 46]. Raman spectra and their deconvoluted counterparts of these three samples are shown in Figure 5. Since the peaks overlap in the original data obtained from Raman spectroscopy, to determine the discrete peaks and obtain the intensities, the diagrams were deconvoluted by Gaussian and Lorentzian functions demonstrating R^2 higher than 0.98. As given in Table 2, the values of I_D/I_G for SiGO and HbpSiGO are meaningfully higher than GO, indicating an increment in the amount of sp3 hybridization of carbon and reduction of sp^2. Allegedly, this can account for the modification process in which reactions between silane molecules and PAMAM occur with GO functionalities.

Table 1: Weight loss and remaining weight of GO, SiGO and HbpSiGO across different temperature ranges.

Sample	Weight loss (%) Up to 150 ºC	Weight loss (%) Up to 300 ºC	Weight loss (%) Up to 500 ºC	Weight loss (%) Up to 700 ºC	Residual Weight at 750 ºC (%)
GO	7.54	46.69	56.76	67.88	29.55
SiGO	0.42	7.56	52.39	60.03	39.27
HbpSiGO	10.09	24.45	43.78	55.04	42.77

Table 2: Data extracted from Raman measurement for GO, SiGO and HbpSiGO.

Sample	GO	SiGO	HbpSiGO
I_D/I_G	0.766	0.930	1.355
I_{2D}/I_G	0.039	0.126	0.195
β	0.0002	0.00035	0.00038

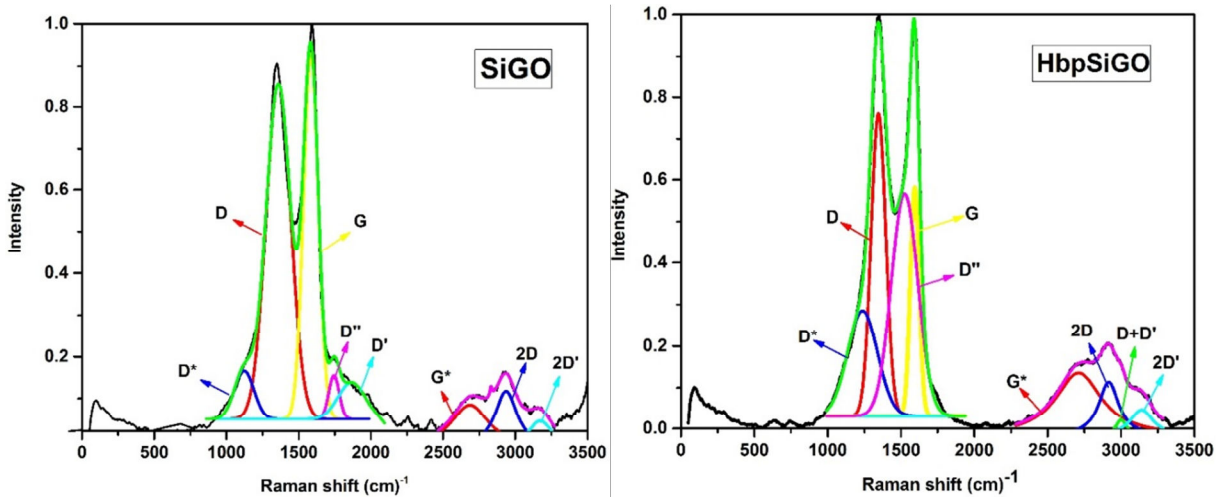

Figure 5: Raman spectra of GO, SiGO and HbpSiGO .

Moreover, the 2D band in the Raman diagram is considered as another essential peak which is appeared around 2830 cm^{-1} for GO. The 2D peak intensity and sharpness are inversely attributed to the number of sheets in the stacks and the interlayer distance of the flakes, i.e., d_{001} [27]. Thus, β as a measure of the peak sharpness and intensity was calculated by dividing the maximum height to the full width at half maximum (FWHM). Moreover, the ratio of I_{2D}/I_G can be considered as an indicator of changes in the interlayer number [27]. According to Table 2, the I_{2D}/I_G for GO is 0.039; however, this ratio for SiGO and HbpSiGO is 0.126 and 0.195, respectively. Thus, as GO is modified, the 2D band becomes sharper, and I_{2D}/I_G ratio increases, indicating a decrease in layers' numbers and an increase in d-spacing between the GO flakes. This event can be considered evidence that the molecules of GPTMS and PAMAM, after diffusion between the layers and GO functionality reacting, have also been able to act as spacing species. The latter is desired since the higher distance between the flakes somehow means an intercalated structure. This change will lead to an enhanced homogenously dispersed morphology in the epoxy resin.

Other characteristic peaks such as D'', D*, and D+D' bands in the Raman spectrum also exist. D* band is correlated to the disordered graphitic lattices of sp^3 carbon, which is virtually observed at 1100-1200 cm^{-1}. In light of the D* position, it can be assumed that shifting D* to a higher wavelength means an increment in oxygen content. As shown in Table 2, D* shifts from 1334 cm^{-1} for GO to 1109 cm^{-1} for SiGO, implying a reduction of oxygen content in GO. It can also be declared that a decrease intensity of D+D' is assigned to the percentage of sp^2 carbon in the modified GO samples [45].

The surface physical chemistry of GO, SiGO, and HbpSiGO was evaluated through contact angle (θ) measurements. Figure 6 demonstrates the measured contact angles of the three samples with a droplet of water. As it is clear, both modified GO samples show a higher contact angle compared to GO inferring an

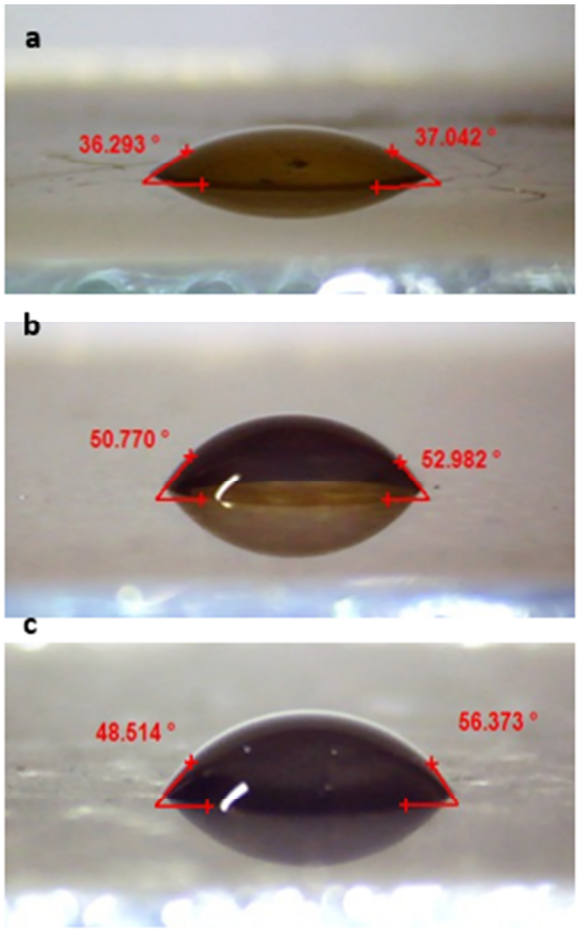

Figure 6: Contact angle of (a) GO, (b) SiGO and (c) HbpSiGO.

increase in hydrophobicity nature of the surface-modified GO samples. This rise is due to the grafting of more hydrophobic structures of GPTMS and PAMAM onto the GO plane. However, it must be noted that HbpSiGO shows smaller θ compared to SiGO, stating that hydrophobicity decreases by PAMAM molecules. This is expected since plenty of relatively hydrophilic amine groups are introduced onto the surface. Such outcome is in complete agreement with the TGA results, which showed a higher amount of adsorbed moisture for this sample. Work of adhesion and surface free energy of the samples were also calculated according to Neumann's (Eq. 1) and Young's (Eq. 2) equations and are shown in Table 3. θ, γ_{lv}, and γ_{sv} are contact angle, liquid surface tension, and the free surface energy of solid, i.e., GO and the modified counterparts. β is a constant and equals 0.0001247 [47].

$$W_A = 2(\gamma_{lv}\gamma_{sv})\exp\left[-\beta(\gamma_{lv}-\gamma_{sv})^2\right] \quad (1)$$

$$W_A = \gamma_{lv}(1+cos\theta) \quad (2)$$

According to Table 3, a decrease in adhesion and surface free energy of the modified GO samples compared to GO occurs, confirming the chemical grafting of the GPTMS and PAMAM molecules on the surface of the GO flakes. Also, this reduction in W_a and γ_{sv} shows that the modified GO is now more compatible with the consequent epoxy resin medium and most probably facilitates particle dispersion and guarantees dispersion relative stability.

The diffraction patterns of GO and its modified counterparts obtained from XRD measurements are displayed in Figure 7. The distinctive diffraction peak of GO appears at a diffraction angle (2θ) of 10.31°, attributed to the interlayer spacing of the basal planes of GO flakes. Using Scherer equation (Eq. 3 and 4), the interlayer distance, i.e. d_{001}, can be calculated [48, 49].

$$L = \frac{0.9\lambda}{B\cos\theta} \quad (3)$$

$$d = \frac{L}{N-1} \quad (4)$$

Table 3: Contact angle, W_A and γ_{sv}.

Sample	GO	SiGO	HbpSiGO
Contact angle (°)	36.66	51.876	52.44
W_A (μJ/cm^2)	12.82	5.549	5.083
γ_{sv} (μJ/cm^2)	13.17	12.246	11.455

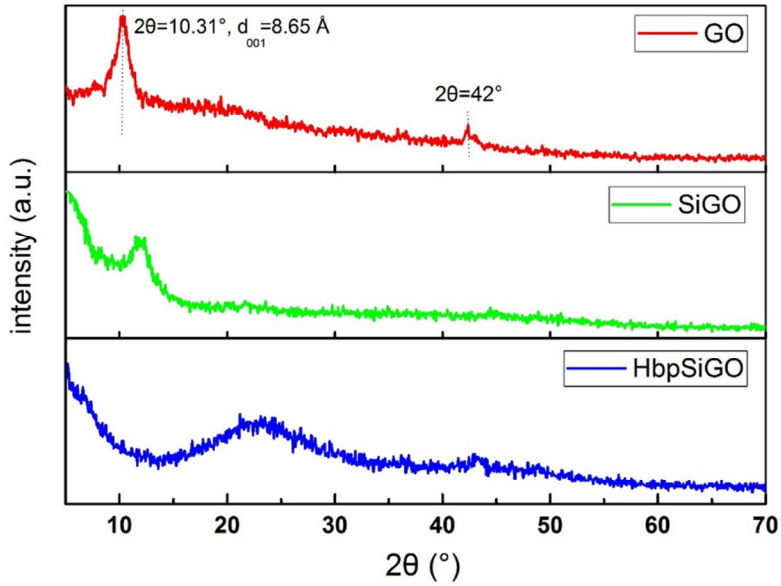

Figure 7: XRD spectra of GO, SiGO and HbpSiGO.

L is the height of stacking of the crystal, λ is the wavelength of the X-ray (0.154 nm), N is layers number, B is FWHM (the full width at the half maximum), and θ is the angle of scattering [41]. The peak calculates the d-spacing for GO at 8.65°. The other peak at a diffraction angle of 42° is attributed to the 321 and 301 planes [50]. However, after surface functionalization, the characteristic peak shifts downwards to lower angles (below 5°) for SiGO and HbpSiGO. Therefore, it seems that the interlayer distance has increased in good accordance with Raman spectroscopy outcomes. This circumstance asserts that GPTMS and PAMAM molecules have penetrated the GO layers and provide an intercalated morphology as desired. Furthermore, the broad peak at around 22° in the HbpSiGO pattern points out that the structure compared with GO has become more amorphous due to the polymer chains-covered GO surfaces.

3.2. Mechanical properties

Stress-strain graphs for epoxy and its nanocomposite counterparts are shown in Figure 8. The quantitative mechanical parameters extracted from these diagrams, including elastic modulus, E, work of fracture, W, elongation at break, ε_{max}, and maximum stress, σ_{max}, are also gathered in Figure 9 and Table 4. E, W, ε_{max}, and σ_{max}, all drastically drop as GO is introduced into the neat epoxy. To explain such behavior, from the molecular interaction point of view, GO can interact with the matrix mainly through hydrogen bonds and Lifshitz-van der Waals forces. However, attraction forces of the GO sheets in stacks are much more vital to be broken by these forces. These unbroken stacks may play stress concentration centers from where the cracks would initiate and propagate. Therefore, such composite structure shows decreased mechanical properties. Also, the negative effect of GO on the curing reactions should also be considered for this deterioration in mechanical performance. However, mechanical behavior becomes different as SiGO is impregnated into the epoxy. The mechanical properties significantly improve in comparison with both neat epoxy, and Ep/GO.

Table 4: Extracted and calculated mechanical parameters of samples from tensile test.

Sample	E (MPa)	W (J)	ε_{max}(%)	σ_{max}(MPa)
neat Ep	2059.2 ± 156	54.14 ± 11	2.345 ± 0.46	37.88 ± 4.4
Ep/GO	1902.4± 65	20.34 ± 7.9	1.716 ± 0.48	25.88 ± 4.1
Ep/SiGO	2504 ± 272	64.96 ± 8.5	2.66 ± 0.58	49.34 ± 2.05
Ep/HbpSiGO	2937.75 ± 220	134.93 ±9.6	3.576 ± 0.03	63.74 ± 3.52

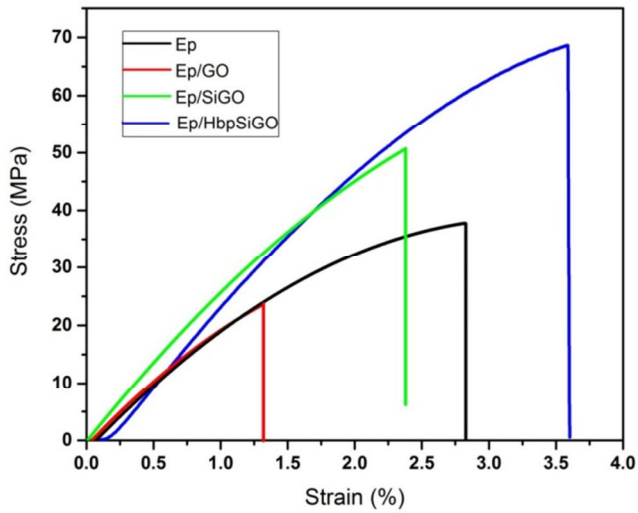

Figure 8: Diagrams of Stress vs. Strain curves of neat and nanocomposite epoxies.

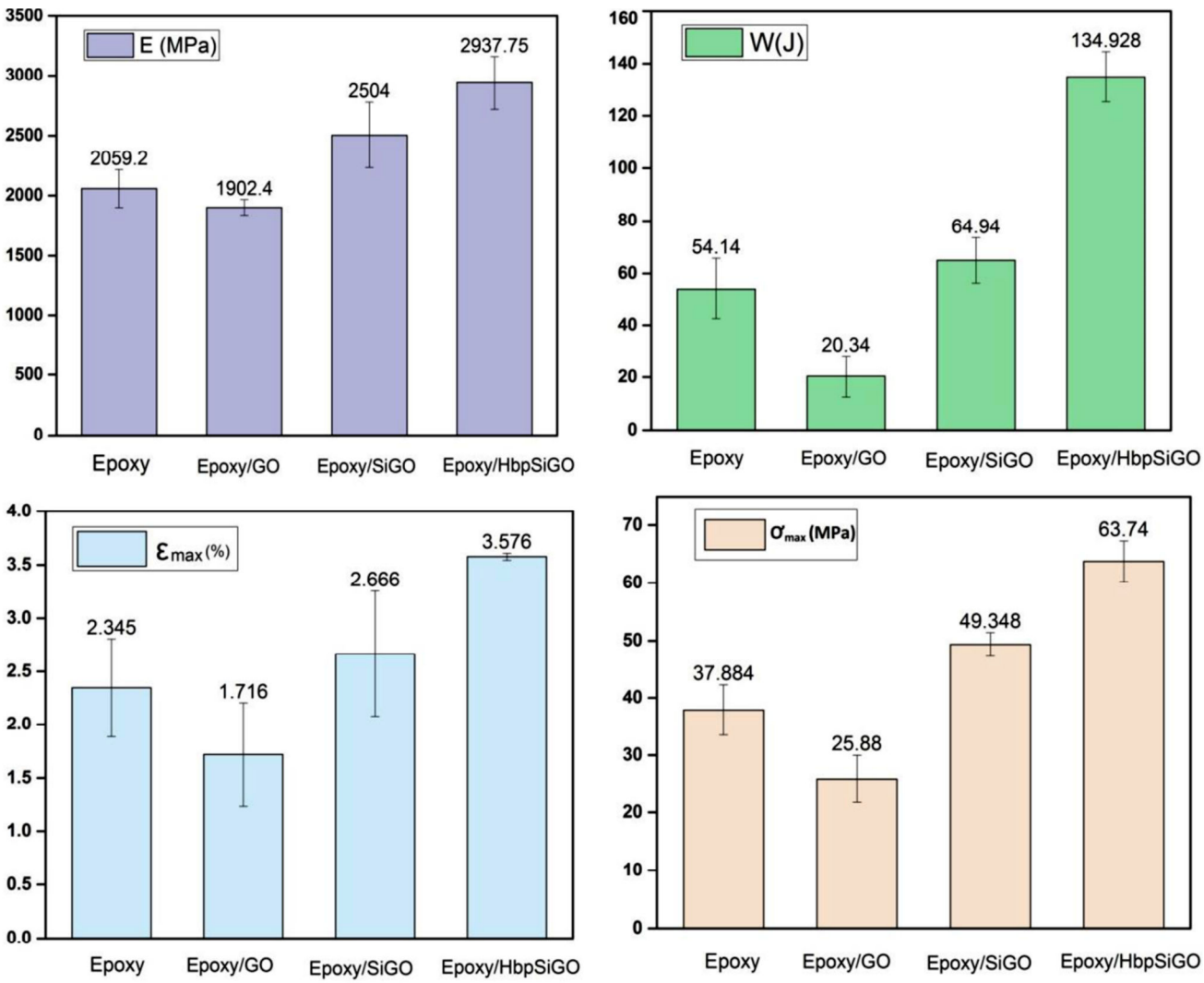

Figure 9: Extracted and calculated mechanical parameters of the samples from tensile test.

Such improvement can also be explained through the molecular interaction between the phases. The silane molecules with terminal epoxide groups can chemically attach to the matrix through covalent reactions with amine groups of the hardener. This linkage, in turn, leads to a much more robust network. Despite the relative lack of proper functional groups on GO surface that can form strong bonds with PAMAM molecules, silane molecules can play a role as a coupling bridge between GO and PAMAM and compensate for the lack of GO proper functional groups. Aside from the possible multitude of interactions between SiGO and PAMAM, the bulky structure of these relatively symmetric spherical molecules prevents the flakes from approaching each other and lowering the possibility of flocculation. This event will lead to a stabilized colloidal system both before and after curing the epoxy medium.

Moreover, the excessive number of terminal amine groups may improve the cross-linking density of the final cure network. That is why Ep/HbpSiGO shows a significant increment in elastic modulus (42 %), work of fracture (148 %), maximum strain (52 %), and maximum stress (68 %) in comparison with neat epoxy. It must also be noted that the hyperbranched polymer possesses dominant elastic nature. Therefore, it induces more elastic deformation, more ductility, and less brittle behavior. A piece of evidence to the latter is that the higher area under the Ep/HbpSiGO shows higher fracture and toughness. As mentioned, the available free NH_2 groups of PAMAM can bond with both terminated epoxide groups of GPTMS and carboxylic acid and epoxide groups of GO.

On the other hand, these big amine groups of PAMAM can also react with the epoxy matrix. These interactions enhance the GO compatibility in the matrix, but the GO dispersion is also increasing. Thus, they prevent the aggregation of GO nanosheets by increasing the distance between GO layers and bonding with the matrix. Furthermore, the network's bonding strength causes a rise in elastic modulus as the highest modulus belongs to Ep/HbpSiGO, which can be quantitatively followed in DMA results by computing cross-linking density of the samples.

Viscoelastic behavior of the samples was further dynamically studied by dynamic mechanical analysis, DMTA. Storage modulus and damping factor as a function of temperature are plotted in Figure 10 for the studied samples. E' at the glassy plateau as a measure of stiffness, E' at the rubbery region as a measure of cross-linking density, and temperature at which E' shows an onset as a measure of the glass transition temperature, i.e., T_g, must be taken into consideration. Also, the maximum Tan's temperature δ emerges as a Tg measure) is an outcome of great importance. These quantitative outcomes have been extracted from the diagrams and represented in Table 5 to compare samples. The storage modulus of Ep/GO nanocomposite in the glassy region decreases by more than 28 % compared to neat epoxy. As it was seen in tensile testing, elastic modulus also showed a reduction in good accordance with storage modulus. This drop can also be similarly explained and attributed to the immiscibility and poor dispersion of GO flakes in the epoxy matrix. Thus, structural inhomogeneity is introduced as the main factor in the deterioration of elastic and storage moduli. However, the modified-GO nanocomposites, notably Ep/HbpSiGO, present higher storage modulus at the glassy region due to the stronger interactions between GO's and epoxy's functional groups, as was mentioned in tensile measurements, which leads to higher stiffness. However, T_g shows a slightly different behavior compared to E' at the glassy region since it goes up by introducing GO particles, both pristine and modified ones.

Table 5: Extracted and Calculated data from the DMA diagrams of the samples.

Sample	T_g (°C)	E' at Glassy Plateau (MPa)	E' at Rubbery Plateau (MPa)	M_e (g/mol)	ν_e (mol/cm^3)
Blank Ep	67.63	1596	9.16	353.71	1033.38
Ep/GO	70.57	1141	8.94	312.26	1042.75
Ep/SiGO	79.96	1895	11.38	292.76	1308.25
Ep/HbpSiGO	72.36	2391.5	30.84	108.78	3486.21

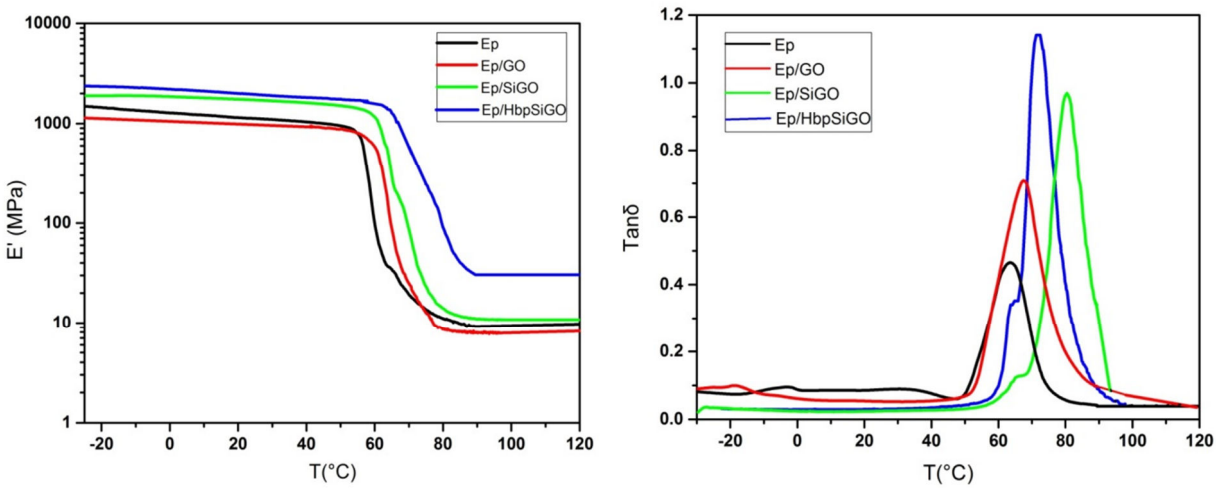

Figure 10: Storage modulus (E') and damping factor (Tanδ) of neat and nanocomposite epoxies.

To explain this behavior, one must consider that T_g is a temperature at which molecular movements start, i.e., approximately 50 atoms of the backbone have a synchronous rotation movement. Additionally, the motion of chains happens through the self-diffusion phenomenon [51]. Introducing GO particles can prevent molecular movement as the temperature increases even though they are dispersed in a non-orderly fashion. GO can induce a decrease in the free volume of the polymer chains and make the diffusion process more difficult. It seems that the inhomogeneity that was responsible for the deterioration of elastic and storage moduli has little effect on T_g.

Furthermore, T_g is also dependent on the network cross-linking density as well. Shorter chains in between the nodes that hinder the motions would increase T_g. Therefore, the molecular weight of the chains between the nodes, consequently the abundance of these nodes per unit volume, i.e., cross-linking density, were calculated by Eq. 5 and 6. These equations, ρ, R, T, E' are polymer density, the universal gas constant, temperature, and minimum storage modulus at the rubbery zone, respectively [51]. The data have been given in Table 5. It is clear that GO, despite the undesired dispersion state in the epoxy matrix, has had meaningful influences on cross-linking density. It is expected because epoxide groups on the GO surface can covalently interact with amine groups of the hardener and increase the number of nodes per unit volume, hence cross-linking density. This result, even more, supports the hypothesis that inhomogeneity is responsible for declining the mechanical properties of Ep/GO. Introducing these nanoparticles into the polymer probably causes a barrier effect to this movement. The hyperbranched polymers and GPTMS, which are connected through the covalent bonds, cause the molecular movements even harder, which results in a relatively significant increase in T_g for Ep/SiGO and Ep/HbpSiGO, i.e., 80 °C (18 % ↑) and 72.4 °C (7 % ↑), respectively. The lower T_g for Ep/HbpSiGO may be correlated to the ball-bearing effect of the spherical molecules of the unreacted PAMAM. The molecular weight of the chain in between the entanglements (M_e) from Eq. 5 and cross-linking density was calculated from Eq. 6.

$$M_e = \frac{\rho RT}{E'} \quad (5)$$

$$\nu_e = \frac{E'}{3RT} \quad (6)$$

As considered the obtained data, a fall in M_e and a rise in ν_e can be seen for the nanocomposites compared to the neat epoxy. On the other hand, an increase of cross-linking density causes the depletion of entropy associated with space structure. It increases the elapsed time for the chain movement (Deborah number), imposing restrictions on the molecular motion of the polymer chain. The observations confirm the explanations above. Other helpful information can be obtained from the Tanδ plot other than T_g. The height of the Tan δ peak indicates the contribution of elastic and viscous parts of the material. The peak's height for Ep/HbpSiGO is the highest, which accounts for the dominant viscous behavior of the polymer chains linking to the GO surface. The morphology of the fractured surface of the neat epoxy and its nanocomposite

counterparts after the tensile test was also studied by a field-emission scanning electron microscope, FE-SEM. These techniques find more evidence for the hypothesis that the mechanical properties and viscoelastic behavior were correlated to the dispersion state of the GO particles inside the epoxy matrix. The images are illustrated in Figure 11. Neat epoxy has a smooth texture with visible cracks, which can be explained in the light of brittle failure and poor resistance of epoxy against crack propagation. By comparison, Ep/GO exhibits a much coarser texture certainly assigned to the aggregation of GO particles. These aggregations can invoke cracks that dissipate work of fracture during the tensile process. There also exist recognizable cavities between the aggregations and epoxy matrix, revealing a tender interfacial attachment between epoxy matrix and GO. Besides, some dimples can also be found on the fractured surface in Ep/GO nanocomposite. The formation of new fractured areas follows the creation of the dimples; thus, much more work of fracture is consumed [52]. Typically these dimples are generated by GO aggregations and can repel crack spreading through branching to encourage the development of many micro-cracks. This event would cause the nanocomposite to consume extra energy during deformation, showing enhanced toughness [53, 54]. It is commonly accepted that nanoparticles cannot contribute to the crack jamming mainly due to the particle dimension, which is much smaller than a dimension of the crack itself [55]. The cracks for Ep/SiGO have deviated that approve the crack diversion mechanism and participate in strengthening nanocomposites impregnated with layered-structured sheets, as suggested by Hull [56]. Ep/HbpSiGO shows fewer rupture lines and a smoother surface with no gap between treated GO and epoxy matrix on the fractured surface on the ground of interface adhesion. The necessary stress for breaking particle aggregations and interfacial attachment between particles and matrix increases, leading to more dissipated fracture energy in conformity with tensile test findings.

3.3. Comparative studies

Few studies are focusing on the surface functionalization of graphene oxide by hyperbranched polymers, which is then used in epoxy polymers to improve the mechanical properties of the resulting nanocomposite. In a study by Jianzhang Li et al. [57], they directly modified GO with an amine-terminated hyperbranched polymer and studied its effect on the improvement of fracture toughness and T_g. They observed enhancement in flexural strength and modulus as high as 41.3 % and 97.3 %, respectively. Another study by Yefa Tan et al. [58] investigated the nanocomposites' curing mechanism and final mechanical properties. They also witnessed an improvement in adhesion and mechanical characteristics. In relatively similar research, Lichun Ma et al. [59] tried to modify carbon fiber by hydroxyl-terminated hyperbranched polymer and then used the modified fiber inside an epoxy matrix. They also improved interfacial shear strength and impact strength from 48.8 MPa and 55.7 kJm^{-2} to 87.8 MPa and 76.9 kJm^{-2}, respectively. In the present study, when HbpSiGO/EP nanocomposite coating is compared with neat epoxy, some significant improvement in physical-mechanical parameters is undeniable, for instance; T_g (18%), work of fracture (148 %), elastic modulus (42 %), and tensile strength (68 %). In other related papers, some improvements have also been reported. Haeri et al. [56] tried to enhance epoxy's mechanical properties by incorporating silica-functionalized GO using TEOS and APTES silane precursors. An increase has been reported in T_g (8 %), W (160 %), E (0.6 %), and tensile strength (32 %) in comparison with neat epoxy. Ghazi Moradi et al. [25] used polyester-amide hyperbranched polymer as a modifier for GO and reported an improvement in T_g (12 %), W (334 %), and tensile strength (48 %) in comparison with neat epoxy. In another research [60], 0.5 wt.% of GO has been reduced with a green, reducing agent and functionalized with Zn^{2+}. They have witnessed an increase in T_g (10 %), E (9 %), and tensile strength (8 %) in comparison with neat epoxy. Chhetri et al. [61] have evaluated the effect of Dodecyal Amine-modified GO on the mechanical parameters and has reported changes in T_g (-21 %), W (60 %), E (38 %), and tensile strength (35 %) of the modified GO/Epoxy composite compared to neat epoxy. Also, some significant improvement in the mechanical parameters such as T_g (12 %), work of fracture (570 %), elastic modulus (54 %), and tensile strength (146 %) is seen for HbpSiGO/EP comparing with GO/EP nanocomposite coating. Haeri et al. [56] reported an increase in T_g (8 %), W (225 %), and tensile strength (64 %), and a decrease in E (-1.2 %) in comparison with GO/epoxy composite. Ghazi Moradi at al. [25] have reported an improvement in T_g (0.7 %), W (2606 %) and tensile strength (137 %) and a decrease in E (-31 %) in comparison with unmodified GO in epoxy.

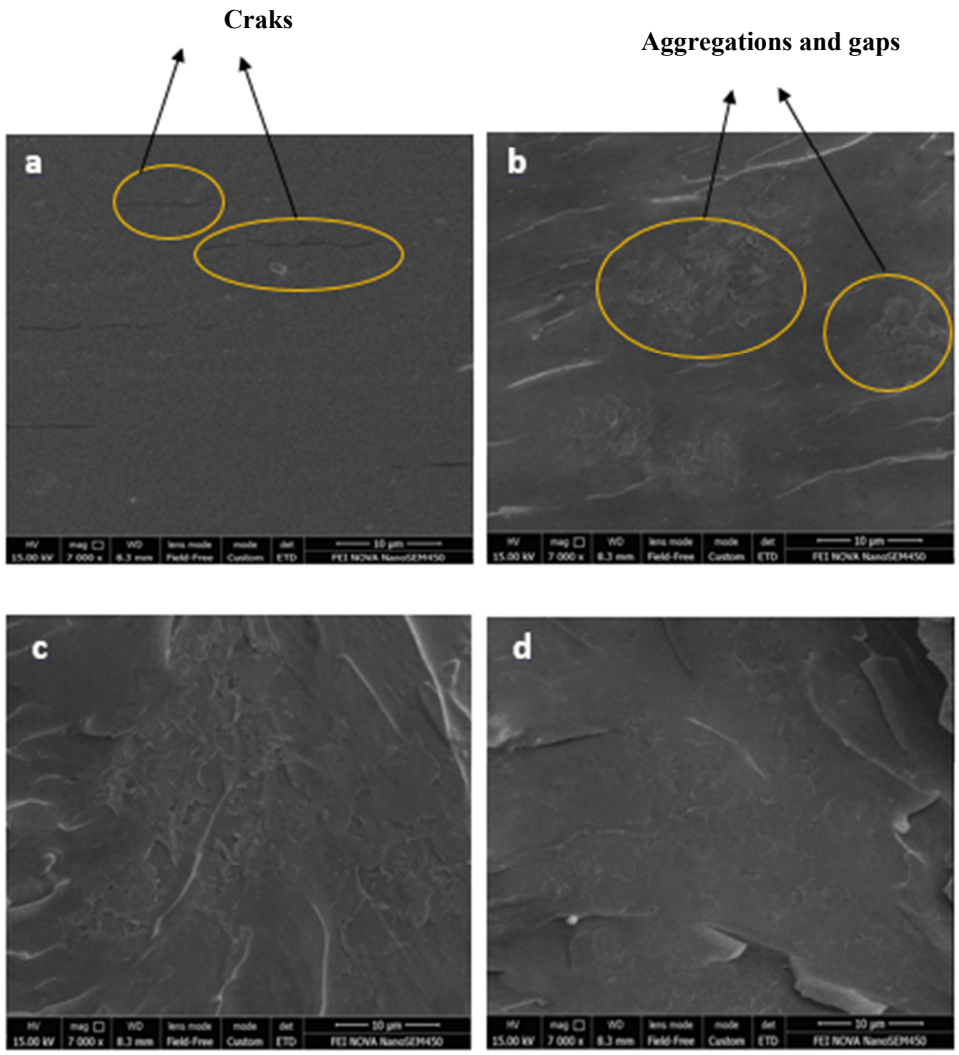

Figure 11: FE-SEM images of fractured cross-section areas of (a) neat Epoxy, (b) Epoxy/GO, (c) Epoxy/SiGO and (d) Epoxy/HbpSiGO.

4. Conclusion

FT-IR, TGA, and Raman spectroscopy measurements show successful grafting of Silane and PAMAM hyperbranched polymers on the GO flakes. The emergence of Si-O-C peak along with Si-O-Si and Si-OH is directly correlated to the silane molecules chemically attached to the functionalities of the GO flakes. Additionally, it is axiomatic that the peak intensity of CH_2 in SiGO has increased due to CH_2 groups of the GPTMS molecules. For HbpSiGO, a peak has emerged at 1560 cm^{-1} representing N-H of the amine groups of PAMAM, proving the existence of PAMAM molecules on the surface of the GPTMS-modified GO. The hydrophilicity of GO declined after modification which was associated with the substitution of more minor hydrophilic functional groups on the GO surface confirmed by measuring the contact angles and surface free energies. The decrease in work of adhesion and surface free energy of the modified GO samples compared with GO demonstrates the chemical grafting of the GPTMS and PAMAM molecules on the surface of the GO flakes. Also, this reduction shows that the modified GO is more compatible with the epoxy resin medium that facilitates particle dispersion and guarantees dispesion relative stability.

XRD analysis indicated an increase in the d-spacing of HbpSiGO due to the diffusion of hyperbranched polymers in between the GO sheets and increasing the interlayer distance because of their bulky structures. GPTMS acted as a coupling agent between GO and PAMAM molecules. Introducing 0.1 wt.% of modified

GO in the epoxy matrix showed remarkable enhanced mechanical properties, including elastic modulus, yield stress, flexibility, and toughness certified by tensile test. Dynamic mechanical analyses showed that the modified-GO nanocomposites, especially Ep/ HbpSiGO, possess higher stiffness and T_g and increased cross-linking density. This result supports the hypothesis that inhomogeneity is responsible for declining the mechanical properties of Ep/GO. Introducing the modified nanoparticles into the polymer causes a barrier effect to this movement. The hyperbranched polymers and GPTMS, which are connected through the covalent bonds, cause the molecular actions even harder, which results in a relatively significant increase in T_g for Ep/SiGO and Ep/HbpSiGO, i.e., 80 °C (18 % ↑) and 72.4 °C (7 % ↑), respectively. Such improvements were assigned to the improved dispersion of modified GO (due to better compatibility) and enhanced interfacial interactions (due to functional groups) between the dispersed and continuous phases. Fe-SEM studies also evidenced the latter hypothesis by correlating the mechanical behavior to the fracture mechanisms of the samples. Conclusively, it can be stated that the modification process designed in this study can somehow remove the mechanical drawbacks of the epoxy matrix.

5. References

1. M. Ramezanzadeh, B. Ramezanzadeh, M. Ganjaee Sari, M.R. Saeb, Corrosion resistance of epoxy coating on mild steel through polyamidoamine dendrimer-covalently functionalized graphene oxide nanosheets, J. *Ind. Eng. Chem*., 82(2020), 290-302.
2. F. Bahremand, T. Shahrabi, B. Ramezanzadeh, Construction of an excellent eco-friendly anti-corrosion system based on epoxy@Sm_2O_3-polydopamine biopolymer on the mild steel surface, *J. Taiwan Inst. Chem. E.*, 113(2020), 332-343.
3. M. Ganjaee Sari, M. Shamshiri, B. Ramezanzadeh, Fabricating an epoxy composite coating with enhanced corrosion resistance through impregnation of functionalized graphene oxide-co-montmorillonite Nanoplatelet, *Corros. Sci*., 129(2017), 38-53.
4. M. Sabu, Y. Jaya Vinse Ruban, P. Raja, S. Ginil Mon, S. Muthukrishnan, Enriched antibacterial and antifouling performance of organoclay filled hybrid epoxy composites, *Compos. Commun*., 24(2021), 100606.
5. C. Bao, Y. Guo, L. Song, Y. Kan, X. Qian, Y. Hu, In situ preparation of functionalized graphene oxide/epoxy nanocomposites with effective reinforcements, *J. Mater. Chem*., 21(2011), 13290-13298.
6. I. Zaman, T.T. Phan, H.C. Kuan, Q. Meng, L.T. Bao La, L. Luong, O. Youssf, J. Ma, Epoxy/graphene platelets nanocomposites with two levels of interface strength, *Polymer (Guildf*), 52(2011), 1603-1611.
7. S. Liu, H. Yan, Z. Fang, Z. Guo, H. Wang, Effect of graphene nanosheets and layered double hydroxides on the flame retardancy and thermal degradation of epoxy resin, *RSC Adv*., 4(2014), 18652-18659.
8. E. Kandare, B.K. Kandola, P. Myler, Evaluating the influence of varied fire-retardant surface coatings on post-heat flexural properties of glass/epoxy composites, *Fire Saf. J*., 58(2013), 112-120.
9. T. H. Ho, C.S. Wang, Modification of epoxy resins with polysiloxane thermoplastic polyurethane for electronic encapsulation: 1, *Polymer (Guildf*)., 37(1996), 2733-2742.
10. M. Wang, L. Ma, B. Li, W. Zhang, H. Zheng, G. Wu, Y. Huang, G. Song, One-step generation of silica particles onto graphene oxide sheets for superior mechanical properties of epoxy composite and scale application, *Compos. Commun*., 22(2020), 100514.
11. Z. Li, R. Wang, R.J. Young, L. Deng, F. Yang, L. Hao, W. Jiao, W. Liu, Control of the functionality of graphene oxide for its application in epoxy nanocomposites, *Polymer (Guildf*)., 54(2013), 6437-6446.
12. L. Rassouli, R. Naderi, M. Mahdavian, Study of the active corrosion protection properties of epoxy ester coating with zeolite nanoparticles doped with organic and inorganic inhibitors, J. *Taiwan Inst. Chem. E.,* 85(2018), 207-220.
13. L. Chen, S. Chai, K. Liu, N. Ning, J. Gao, Q. Liu, F. Chen, Q. Fu, Enhanced epoxy/silica composites mechanical properties by introducing graphene oxide to the interface, *ACS Appl. Mater. Interfaces*., 4(2012), 4398-4404.
14. C. L. Poh, M. Mariatti, M.N. Ahmad Fauzi, C.H. Ng, C.K. Chee, T.P. Chuah, Tensile, dielectric, and thermal properties of epoxy composites filled with silica, mica, and calcium carbonate, J. *Mater. Sci. Mater. Electron*., 25(2014), 2111-2119.
15. T. H. Wu, A. Foyet, A. Kodentsov, L.G.J. van der Ven, R.A.T.M. van Benthem, G. de With, Curing and percolation for carbon black-epoxy-amine nanocomposites, *Compos. Sci. Technol*., 181(2019), 107672.
16. J. He, H. Wang, Q. Qu, Z. Su, T. Qin, Y. Da, X. Tian, Self-assembled three-dimensional structure with optimal ratio of GO and SiC particles effectively improving the thermal conductivity and reliability of epoxy composites, *Compos. Commun*., 22(2020), 100448.

17. A. A. Javidparvar, B. Ramezanzadeh, E. Ghasemi, The effect of surface morphology and treatment of Fe_3O_4 nanoparticles on the corrosion resistance of epoxy coating, *J. Taiwan Inst. Chem. E.,* 61(2016), 356-366.
18. C. Liu, J. Li, Z. Jin, P. Hou, H. Zhao, L. Wang, Synthesis of graphene-epoxy nanocomposites with the capability to self-heal underwater for materials protection, *Compos. Commun*., 15(2019), 155-161.
19. Y. Yuan, Y.T. Pan, Z. Zhang, R. Yang, Temperature-tuned dimensional transition of graphitic nanoparticles and its effect on the fire safety of epoxy nanocomposites, *Compos. Commun*., 22(2020), 100488.
20. B. P. Singh, B.K. Jena, S. Bhattacharjee, L. Besra, Development of oxidation and corrosion resistance hydrophobic graphene oxide-polymer composite coating on copper, *Surf. Coatings Technol*., 232(2013), 475-481.
21. H. Di, Z. Yu, Y. Ma, C. Zhang, F. Li, L. Lv, Y. Pan, H. Shi, Y. He, Corrosion-resistant hybrid coatings based on graphene oxide–zirconia dioxide/epoxy system, *J. Taiwan Inst. Chem. E*., 67(2016), 511-520.
22. B. Ramezanzadeh, B. Karimi, M. Ramezanzadeh, M. Rostami, Synthesis and characterization of polyaniline tailored graphene oxide quantum dot as an advance and highly crystalline carbon-based luminescent nanomaterial for fabrication of an effective anti-corrosion epoxy system on mild steel, *J. Taiwan Inst. Chem. E*., 95(2019), 369-382.
23. M. Ganjaee Sari, B. Ramezanzadeh, A.S. Pakdel, M. Shahbazi, A physico-mechanical investigation of a novel hyperbranched polymer-modified clay/epoxy nanocomposite coating, *Prog. Org. Coat*., 99(2016), 263-273.
24. F. Mirshahi, S. Bastani, M. Ganjaee Sari, Studying the effect of hyperbranched polymer modification on the kinetics of curing reactions and physical/mechanical properties of UV-curable coatings, *Prog. Org. Coatings*., 90(2016), 187-199.
25. L. Ghazi Moradi, M. Ganjaee Sari, B. Ramezanzadeh, Polyester-amide hyperbranched polymer as an interfacial modifier for graphene oxide nanosheets: Mechanistic approach in an epoxy nanocomposite coating, *Prog. Org. Coat*., 142(2020), 105573.
26. M. Abdolmaleki, M. Ganjaee Sari, M. Rostami, B. Ramezanzadeh, Graphene oxide nanoflakes as an efficient dispersing agent for nanoclay lamellae in an epoxy-phenolic nanocomposite coating: Mechanistic approach, *Compos. Sci. Technol*., 184(2019), 107879.
27. M. G. Sari, M. Abdolmaleki, M. Rostami, B. Ramezanzadeh, Nanoclay dispersion and colloidal stability improvement in phenol novolac epoxy composite via graphene oxide for the achievement of superior corrosion protection performance, *Corros. Sci*., 173(2020), 108799.
28. M. Ganjaee Sari, B. Ramezanzadeh, M. Shahbazi, A.S. Pakdel, Influence of nanoclay particles modification by polyester-amide hyperbranched polymer on the corrosion protective performance of the epoxy nanocomposite, *Corros. Sci*., 92(2015), 162-172.
29. M. Ganjaee Sari, H. Vahabi, X. Gabrion, P. Laheurte, P. Zarrintaj, K. Formela, M.R. Saeb, An attempt to mechanistically explain the viscoelastic behavior of transparent epoxy/starch-modified ZnO nanocomposite coatings, *Prog. Org. Coat*., 119(2018), 171-182.
30. M. Ganjaee Sari, M. Shahbazi, A.S. Pakdel, Developing a novel hyperbranched polymer-modified PP/Clay nanocomposite: characteristics investigation, *Polym. - Plast. Technol. Eng*., 53(2014), 1561-1573.
31. M. G. Sari, B. Ramezanzadeh, Epoxy composite coating corrosion protection properties reinforcement through the addition of hydroxyl-terminated hyperbranched polyamide non-covalently assembled graphene oxide platforms, *Constr. Build. Mater*., 234(2020), 117421.
32. B. Ramezanzadeh, S. Niroumandrad, A. Ahmadi, M. Mahdavian, M.H. Mohamadzadeh Moghadam, Enhancement of barrier and corrosion protection performance of an epoxy coating through wet transfer of amino functionalized graphene oxide, *Corros. Sci*., 103(2016), 283-304.
33. M. Fang, Z. Zhang, J. Li, H. Zhang, H. Lu, Y. Yang, Constructing hierarchically structured interphases for strong and tough epoxy nanocomposites by amine-rich graphene surfaces, *J. Mater. Chem*., 20 (2010), 9635-9643.
34. M. Cano, U. Khan, T. Sainsbury, A. O'Neill, Z. Wang, I.T. McGovern, W.K. Maser, A.M. Benito, J.N. Coleman, Improving the mechanical properties of graphene oxide based materials by covalent attachment of polymer chains, *Carbon*., 52(2013), 363-371.
35. S. Hou, S. Su, M.L. Kasner, P. Shah, K. Patel, C.J. Madarang, Formation of highly stable dispersions of silane-functionalized reduced graphene oxide, *Chem. Phys. Lett.,* 501(2010), 68-74.
36. W. S. Ma, J. Li, X.S. Zhao, Improving the thermal and mechanical properties of silicone polymer by incorporating functionalized graphene oxide, *J. Mater. Sci.*, 48(2013), 5287-5294.
37. T. Jiang, T. Kuila, N.H. Kim, B.C. Ku, J.H. Lee, Enhanced mechanical properties of silanized silica nanoparticle attached graphene oxide/epoxy composites, *Compos. Sci. Technol*., 79(2013), 115-125.
38. M. Nonahal, H. Rastin, M.R. Saeb, M.G. Sari, M.H. Moghadam, P. Zarrintaj, B. Ramezanzadeh, Epoxy/PAMAM dendrimer-modified graphene oxide nanocomposite coatings: Nonisothermal cure kinetics study, *Prog. Org. Coat*., 114(2018), 233-243.
39. M. Maadani, H. Jafari, M.R. Saeb, B. Ramezanzadeh, F. Najafi, D. Puglia, Studying the corrosion protection behavior of an epoxy composite coating reinforced with functionalized graphene oxide by second and

fourth generations of poly(amidoamine) dendrimers (GO-PAMAM-2, 4), *Prog. Color. Colorant Coat*., 13(2020), 261-273.
40. S. Musić, N. Filipović-Vinceković, L. Sekovanić, Precipitation of amorphous SiO_2 particles and their properties, Brazilian *J. Chem. Eng*., 28(2011), 89-94.
41. P. Liu, Z. Yao, L. Li, J. Zhou, In situ Synthesis and mechanical, thermal properties of polyimide nanocomposite film by addition of functionalized graphene oxide, *Polym. Compos*., 37(2016), 907-914.
42. C. Y. Lee, J.H. Bae, T. Y. Kim, S. H. Chang, S. Y. Kim, Using silane-functionalized graphene oxides for enhancing the interfacial bonding strength of carbon/epoxy composites, Compos. Part A Appl. Sci. Manuf., 75(2015), 11-17.
43. L. Kou, C. Gao, Making silica nanoparticle-covered graphene oxide nanohybrids as general building blocks for large-area superhydrophilic coatings, Nanoscale., 3(2011), 519-528.
44. P. Liu, Z. Yao, J. Zhou, Controllable synthesis and enhanced microwave absorption properties of silane-modified $Ni_{0.4}Zn_{0.4}Co_{0.2}Fe_2O_4$ nanocomposites covered with reduced graphene oxide, *RSC Adv.,* 5(2015), 93739-93748.
45. D. López-Díaz, M. López Holgado, J.L. García-Fierro, M.M. Velázquez, Evolution of the raman spectrum with the chemical composition of graphene oxide, *J. Phys. Chem. C.,* 121(2017), 20489-20497.
46. S. Claramunt, A. Varea, D. López-Díaz, M.M. Velázquez, A. Cornet, A. Cirera, The importance of interbands on the interpretation of the raman spectrum of graphene oxide, *J. Phys. Chem. C.,* 119(2015), 10123-10129.
47. B. Manoj, A.G. Kunjomana, Study of stacking structure of amorphous carbon by X-Ray diffraction technique, *Int. J. Electrochem. Sci*., 7(2012), 3127-3134.
48. B.K. Saikia, R.K. Boruah, P.K. Gogoi, A X-ray diffraction analysis on graphene layers of Assam coal, *J. Chem. Sci*., 121(2009), 103-106.
49. V. Reddy, K.K.C. Satish Babu, S.R. Torati, Y.J. Eom, T.Q. Trung, N.E. Lee, C. G. Kim, Scalable production of water-dispersible reduced graphene oxide and its integration in a field effect transistor, *J. Ind. Eng. Chem.,* 63(2018), 19-26.
50. N. T. Qazvini, N. Mohammadi, Dynamic mechanical analysis of segmental relaxation in unsaturated polyester resin networks: Effect of styrene content, *Polymer (Guildf),* 46(2005), 9088-9096.
51. N. Wu, X. She, D. Yang, X. Wu, F. Su, Y. Chen, Synthesis of network reduced graphene oxide in polystyrene matrix by a two-step reduction method for superior conductivity of the composite, *J. Mater. Chem.,* 22(2012), 17254-17261.
52. D. R. Bortz, E. G. Heras, I. Martin-Gullon, Impressive fatigue life and fracture toughness improvements in graphene oxide/epoxy composites, *Macromolecules*., 45(2012), 238-245.
53. P. C. Ma, J. K. Kim, B. Z. Tang, Effects of silane functionalization on the properties of carbon nanotube/epoxy nanocomposites, *Compos. Sci. Technol.,* 67(2007), 2965-2972.
54. B. B. Johnsen, A.J. Kinloch, R. D. Mohammed, A. C. Taylor, S. Sprenger, Toughening mechanisms of nanoparticle-modified epoxy polymers, *Polymer* (Guildf), 48(2007), 530-541.
55. S. Z. Haeri, M. Asghari, B. Ramezanzadeh, Progress in Organic Coatings Enhancement of the mechanical properties of an epoxy composite through inclusion of graphene oxide nanosheets functionalized with silica nanoparticles through one and two steps sol-gel routes, *Prog. Org. Coat.,* 111(2017), 1-12.
56. D. Hull, Fractography: observing, measuring and interpreting fracture surface topography, Cambridge University Press, 1st edition, 1999.
57. J. Li, W. Zhu, S. Zhang, Q. Gao, J. Li, W. Zhang, Amine-terminated hyperbranched polyamide covalent functionalized graphene oxide-reinforced epoxy nanocomposites with enhanced toughness and mechanical properties, *Polym. Test*., 76(2019), 232-244.
58. Z. Qi, Y. Tan, L. Gao, C. Zhang, L. Wang, C. Xiao, Effects of hyperbranched polyamide functionalized graphene oxide on curing behaviour and mechanical properties of epoxy composites, *Polym. Test.,* 71(2018), 145-155.
59. L. Shi, L. Ma, P. Li, M. Wang, S. Guo, P. Han, G. Song, The effect of self-synthesized hydroxyl-terminated hyperbranched polymer interface layer on the properties of carbon fiber reinforced epoxy composites, *Appl. Surf. Sci.,* 479(2019), 334-343.
60. S. Saadatmandi, M. Asghari, B. Ramezanzadeh, Effective epoxy composite coating mechanical/ fracture toughness properties improvement by incorporation of graphene oxide nano-platforms reduced by a green / biocompataible reductant, *J. Ind. Eng. Chem.*, 75 (2019), 271-284.
61. S. Chhetri, P. Samanta, N.C. Murmu, S.K. Srivastava, T. Kuila, Effect of dodecyal amine functionalized graphene on the mechanical and thermal properties of epoxy-based composites, *Poly. Eng. Sci*., (2016), 1-8.

How to cite this article:
M. Ganjaee Sari, M. Rostami, S. Khamseh, Poly(amidoamine)-grafted Graphene Oxide/Epoxy Nanocomposite: Thermal/Mechanical Characteristics and Viscoelastic Properties. Prog. Color Colorants Coat., 15 (2022), 157-174.